Fundamental Saliency based Encoderless Control for Reluctance Synchronous Machines

P. Landsmann and R. Kennel, *Senior, IEEE*

Electrical Drive Systems and Power Electronics
Technische Universitaet Muenchen, Germany

H.W. de Kock and M.J. Kamper, *Senior, IEEE*

Electrical Machines Laboratory
Stellenbosch University, South Africa

***Abstract*—This paper presents a rotor position estimation and sensorless control scheme for reluctance synchronous machines for medium to high speed. The position information is obtained from the fundamental saliency of the machine. First a linear estimation scheme is derived in theory and then extended for the nonlinear effects in a real machine. Finally the performance of the proposed scheme is proved by stationary and dynamic measurements.**

I. Introduction

As the principle of torque production in reluctance synchronous machines (RSMs) relinquishes the need for copper or permanent magnets in the rotor, whereas its efficiency and power density can be comparable to induction machines [1]–[3], RSMs are especially suitable for low cost applications and receiving more and more attention in this field. Furthermore the RSM itself is very robust against harsh environmental conditions with one exception: a position sensor is needed for control. This sensor and the related circuitry also markedly raises the cost of the entire system. Furthermore, in low cost applications the accuracy of the position normally is a minor concern. For all the above reasons it is reasonable to consider controlling the RSM without a position sensor for certain applications, e.g. fans and pumps [1].

The torque production of the RSM is based on a strong rotor fixed fundamental saliency. The fundamental saliency describes the phenomenon that the amount of flux per current depends on the current angle. Despite the fundamental saliency it is common to use saliency referring to the angle dependent inductance of the machine, particularly regarding high frequency injection based sensorless control methods [1], [4]–[9] which are based on the inductance saliency. In the linear case both salincies are identical, whereas in the nonlinear case they are connected by a differential relation, which is exemplified in Fig. 1.

Except conditions of heavy saturation a fundamental saliency consequently results in an inductance saliency, which makes the RSM obviously suited well for high frequency injection based rotor position estimation methods. Theses approaches can be separated in rotating voltage injection [4], alternating voltage injection [1], [5]–[7] or pulse injection [8], [9].

However, under certain operating conditions with heavy saturation high frequency methods are at risk of failing, since the inductance saliency can become very small, even if the fundamental saliency retains its strength. Furthermore to apply the high frequency excitation additional voltage margin is required, so those schemes are only feasibly up to medium speeds.

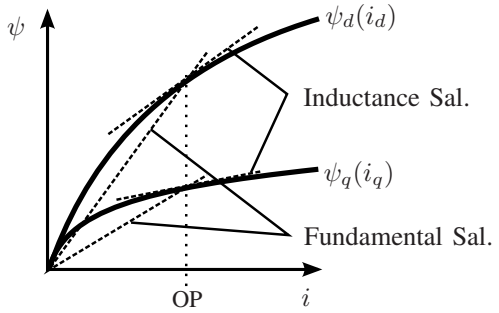

Fig. 1. Fundamental and inductance saliency

Commonly for permanent magnet or wound rotor synchronous motors a fundamental excitation based sensorless scheme [10], [11] takes over from medium to high speed. These schemes estimate the direction of the rotor flux, which is supposed to be equal to the rotor position, by observing the EMF. But unlike these machines, the RSM has no rotor own source of flux: the flux is caused only by the stator currents. As a consequence usual EMF based rotor position estimation methods cannot be used for the RSM.

Few fundamental model based approaches for sensorless control of the RSM have been published [12]–[14]. The work in [12] describes a mathematical approach to use the first harmonic of the rotor position. In [13] only the flux position and not the rotor position is estimated. Evaluating the rotor position estimation scheme of [14] it appears to become unstable for certain current angles within the operating region.

The approach proposed in this paper shares its basis thought with [14] but concludes to a different scheme which is stable for all current angles within the operating region. Since the fundamental saliency has to be calculated using integration of the fundamental voltage, the performance of the proposed scheme improves with raising rotor speed.

After deriving a linear scheme in theory and extending it regarding the nonlinear effects of the machine, the proposed scheme is analysed and validated using experimental results.

978-1-4244-4175-4/10/$25.00 ©2010 IEEE

A. Nomenclature and Definitions

Symbols:

$u,\ i,\ \psi$	voltage, current and flux linkage
$R,\ L$	resistance and inductance
Y	inverse inductance
$M,\ \Theta$	mechanical torque and inertia
$\theta,\ \omega$	electrical rotor angle and speed

Indices:

$s,\ r$	stator and rotor
a, b, c	stator phase axes
$\alpha,\ \beta$	stator fixed cartesian axes
$d,\ q$	rotor fixed direct and quadrature axes

Scalar values are written in normal letters, e.g. R or τ, vector values ($\mathbb{R}^2$) are written in bold small letters, e.g. $\boldsymbol{i}$ or $\boldsymbol{\psi}$, and tensors or matrices ($\mathbb{R}^{2\times2}$) are written in bold capital letters, e.g. $\mathbf{L}$ or $\mathbf{T}^{-1}$.

Subscripts describe the location of the physical quantity, e.g. R_s is the resistance of the stator windings. The superscript specifies the used reference frame, e.g. $\boldsymbol{i}_s^r$ is the stator current vector in rotor fixed reference frame. Thus scalar values will not have a superscript. The superscript ^{T} is used to transpose a vector or a matrix and the superscript $^{-1}$ for the inverse.

Transforms of vectors from one reference frame into another, i.e. vector rotations are done by using the rotor angle dependent matrix $\mathbf{T}$ ($r \rightarrow s$) or $\mathbf{T}^{-1}$ ($s \rightarrow r$) respectively.

$$\mathbf{T} = \begin{bmatrix} \cos\theta & -\sin\theta \\ \sin\theta & \cos\theta \end{bmatrix} \tag{1}$$

$$\mathbf{T}^{-1} = \begin{bmatrix} \cos\theta & \sin\theta \\ -\sin\theta & \cos\theta \end{bmatrix} \tag{2}$$

An orthogonal rotation is done by the constant matrix $\mathbf{J}$.

$$\mathbf{J} = \mathbf{T}\left(\tfrac{\pi}{2}\right) = \begin{bmatrix} 0 & -1 \\ 1 & 0 \end{bmatrix} \tag{3}$$

$\mathbf{T}$ and $\mathbf{J}$ are the vector equivalents to the complex operators $e^{j\theta}$ and j respectively.

Derivatives with respect to time are indicated by a dot, e.g. $\dot{\boldsymbol{i}}_s^s$ or $\dot{\mathbf{L}}_s^s$ and derivatives with respect to the rotor angle by a prime, e.g. $\mathbf{T}^{-1\prime}$ or $\mathbf{L}_s^{s\prime}$.

II. RSM Basic Operation

The cross section of the used RSM is shown in Fig. 2. This transverse laminated motor has two pole pairs and distributed stator windings. The rotor is characterised by a large saliency due to the flux barriers: the d-axis is in the direction of maximum permeance and the q-axis is aligned crossing the flux barriers. For very low currents the magnitudes of the flux in d- and in q-axis are nearly the same (see the measured results in Fig. 7). In order to make the saliency measurable in the stator currents (to make the saliency "visible"), it is necessary to always apply a small q-axis current of $0.8A$, just enough to saturate the q-axis. No torque is generated

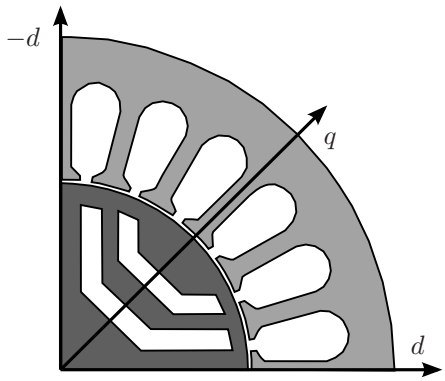

Fig. 2. Cross section of the used RSM

when only q-axis current is applied. In [15] it is showed that the maximum torque per current locus for this RSM can be approximated by a constant current angle of 60^o. Since it is both important to make the saliency visible and to have maximum torque per current, it is now proposed to apply $0.8A$ q-axis current for a zero torque reference and to approach the 60^o current angle point for maximum torque, as shown in Fig. 3. This line defines all the target operating points of the RSM. No special care is taken for the field weakening region, i.e. to advance the current angle towards the q-axis as usual [14]. It is argued that the field weakening range is rather limited anyway due to motor properties, so the RSM should in general not be used for applications that require large field weakening ranges, and therefore the control also doesn't need to be optimised for that operating region.

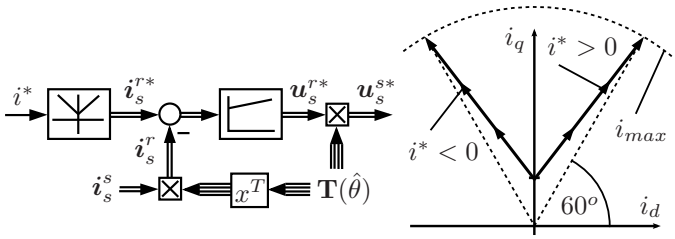

Fig. 3. Current Control of RSM

As shown in 3, the usual current vector control in the rotor fixed reference frame is performed, typically referred to as field oriented control (FOC). In the encoderless case, the estimation position (as opposed to the measured rotor position) is used to transform the measured stator currents into the estimated rotor fixed reference frame, and transform the output voltage of the current regulator back to the stationary reference frame.

III. General Mathematical Model of the RSM

The stator voltage equation (4) is:

$$\boldsymbol{u}_s^s = R_s \boldsymbol{i}_s^s + \dot{\boldsymbol{\psi}}_s^s \tag{4}$$

The flux linkage $\boldsymbol{\psi}_s^s$ of the RSM is only caused by the stator currents and varied in magnitude and orientation as a function

of the the rotor angle.

$$\boldsymbol{\psi}_s^s = \boldsymbol{\psi}_s^s\left(\boldsymbol{i}_s^s, \theta\right) \tag{5}$$
$$= \mathbf{T}\boldsymbol{\psi}_s^r\left(\boldsymbol{i}_s^r\right) \tag{6}$$
$$= \mathbf{T}\boldsymbol{\psi}_s^r\left(\mathbf{T}^{-1}\boldsymbol{i}_s^s\right) \tag{7}$$

The function $\boldsymbol{\psi}_s^r\left(\boldsymbol{i}_s^r\right)$ is a one-to-one assignment of a current vector to a flux linkage vector in rotor fixed frame. It can be linear or nonlinear but for an RSM it has to be anisotropic. Equation (4) requires the derivation of (7) with respect to the time.

$$\dot{\boldsymbol{\psi}}_s^s = \frac{\partial \mathbf{T}}{\partial \theta}\frac{d\theta}{dt}\boldsymbol{\psi}_s^r + \mathbf{T}\frac{\partial \boldsymbol{\psi}_s^r}{\partial \boldsymbol{i}_s^r}\frac{d\boldsymbol{i}_s^r}{dt} \tag{8}$$
$$= \mathbf{L}_s^s\dot{\boldsymbol{i}}_s^s + \mathbf{J}\omega\boldsymbol{\psi}_s^s - \mathbf{L}_s^s\mathbf{J}\omega\boldsymbol{i}_s^s \tag{9}$$
$$\text{with} \quad \mathbf{L}_s^s = \mathbf{T}\mathbf{L}_s^r\mathbf{T}^{-1} \quad \text{and} \quad \mathbf{L}_s^r = \frac{\partial \boldsymbol{\psi}_s^r}{\partial \boldsymbol{i}_s^r} \tag{10}$$

Using (10) the voltage equation (4) can be transposed to calculate the current derivative $\dot{\boldsymbol{i}}_s^s$.

$$\dot{\boldsymbol{i}}_s^s = \mathbf{L}_s^{s\,-1}\left(\boldsymbol{u}_s^s - R_s\boldsymbol{i}_s^s - \mathbf{J}\omega\boldsymbol{\psi}_s^s + \mathbf{L}_s^s\mathbf{J}\omega\boldsymbol{i}_s^s\right) \tag{11}$$

The vector product of current and flux linkage gives the torque M of the machine.

$$M = \frac{3p}{2}\;\boldsymbol{i}_s^{s\;T}\;\mathbf{J}\;\boldsymbol{\psi}_s^s \tag{12}$$

IV. Linear Position Estimator

A. Linearisation of the Model of the RSM

The flux linkage in rotor fixed frame $\boldsymbol{\psi}_s^r$ is assumed to have a linear dependency on the current in rotor fixed frame $\boldsymbol{i}_s^r$, i.e. the value of the flux linkage can just be calculated using the inductance $\mathbf{L}_s^r$.

$$\boldsymbol{\psi}_s^r\left(\boldsymbol{i}_s^r\right) = \mathbf{L}_s^r\boldsymbol{i}_s^r \tag{13}$$

Since the rotor is still anisotropic the inductance remains a tensor that is constant in rotor fixed frame.

$$\mathbf{L}_s^r = \begin{bmatrix} L_d & 0 \\ 0 & L_q \end{bmatrix} \tag{14}$$
$$\mathbf{L}_s^s = \mathbf{T}\mathbf{L}_s^r\mathbf{T}^{-1} \tag{15}$$
$$= \begin{bmatrix} L_d\cos^2\theta + L_q\sin^2\theta & (L_d - L_q)\sin\theta\cos\theta \\ (L_d - L_q)\sin\theta\cos\theta & L_d\sin^2\theta + L_q\cos^2\theta \end{bmatrix} \tag{16}$$

By introducing L_Σ and L_Δ the inductance in stator fixed frame (16) can be rewritten using an isotropic and a rotating term.

$$L_\Sigma = \frac{L_d + L_q}{2} \qquad L_\Delta = \frac{L_d - L_q}{2} \tag{17}$$
$$\mathbf{L}_s^s = L_\Sigma\begin{bmatrix} 1 & 0 \\ 0 & 1 \end{bmatrix} + L_\Delta\begin{bmatrix} cos(2\theta) & sin(2\theta) \\ sin(2\theta) & -cos(2\theta) \end{bmatrix} \tag{18}$$

B. Position Estimation Technique

Using (18) the resulting flux linkage in stator fixed frame $\boldsymbol{\psi}_s^s$ from (13) can be separated in $\boldsymbol{\psi}_\Sigma^s$ and $\boldsymbol{\psi}_\Delta^s$.

$$\boldsymbol{\psi}_s^s = L_\Sigma\boldsymbol{i}_s^s + L_\Delta\begin{bmatrix} cos(2\theta) & sin(2\theta) \\ sin(2\theta) & -cos(2\theta) \end{bmatrix}\boldsymbol{i}_s^s \tag{19}$$
$$= \boldsymbol{\psi}_\Sigma^s + \boldsymbol{\psi}_\Delta^s \tag{20}$$

As indicated in Fig. 4 $\boldsymbol{\psi}_\Sigma^s$ is parallel to the current and $\boldsymbol{\psi}_\Delta^s$ rotates with double rotor speed while having constant magnitude. θ_i is the angle between the current and the rotor d-axis.

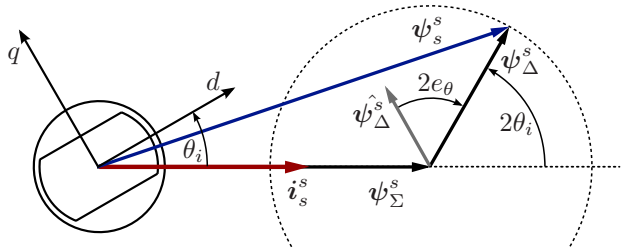

Fig. 4. Flux linkage orientation due to saliency

If L_d and L_q are known and $\boldsymbol{i}_s^s$ is measured one can easily shift the circle to the origin by the following subtraction.

$$\boldsymbol{\psi}_\Delta^s = \boldsymbol{\psi}_s^s - L_\Sigma\boldsymbol{i}_s^s \tag{21}$$
$$= \int \boldsymbol{u}_s^s - R_s\boldsymbol{i}_s^s\;dt - L_\Sigma\boldsymbol{i}_s^s \tag{22}$$

Thus $\boldsymbol{\psi}_\Delta^s$ is a rotating vector that can be calculated from measured quantities. It can also be estimated using the angle $\hat{\theta}$ of a phase locked loop (PLL) structure.

$$\hat{\boldsymbol{\psi}}_\Delta^s = \mathbf{S}(\theta)\boldsymbol{i}_s^s = \begin{bmatrix} cos(2\hat{\theta}) & sin(2\hat{\theta}) \\ sin(2\hat{\theta}) & -cos(2\hat{\theta}) \end{bmatrix}\boldsymbol{i}_s^s \tag{23}$$

The vector product of $\boldsymbol{\psi}_\Delta^s$ and $\hat{\boldsymbol{\psi}}_\Delta^s$ can be used to determine an angle difference between both vectors and fed back to the PLL as the error signal in order to drive its deviation to zero.

$$e_{pll} = \boldsymbol{\psi}_\Delta^{s\;T}\mathbf{J}\;\hat{\boldsymbol{\psi}}_\Delta^s \tag{24}$$
$$= |\boldsymbol{\psi}_\Delta^s|\left|\hat{\boldsymbol{\psi}}_\Delta^s\right| sin(2e_\theta), \quad e_\theta = \theta - \hat{\theta} \tag{25}$$

As shown in Fig. 4, $\boldsymbol{\psi}_\Delta^s$ and $\hat{\boldsymbol{\psi}}_\Delta^s$ will not have the same length as the factor L_Δ was neglected in (23). Since the length of the vectors simply acts like a gain in the PLL error and the gains of the PLL controller have to be adjusted anyway, neglecting it will not cause an estimation error.

But this fact leads to an advantage regarding the drift problems of the flux calculation by voltage integration using (22) only: As consequently also the length of $\boldsymbol{\psi}_\Delta^s$ does not matter, it is possible to yield a drift compensation without affecting the angle estimation by smoothly pulling $\boldsymbol{\psi}_s^s$ towards $\boldsymbol{\psi}_\Sigma^s$. This can be achieved by subtracting $k_d\boldsymbol{\psi}_\Delta^s$ within the integral of equation (22).

$$\boldsymbol{\psi}_\Delta^s = \int \boldsymbol{u}_s^s - R_s\boldsymbol{i}_s^s - k_d\boldsymbol{\psi}_\Delta^s\;dt - L_\Sigma\boldsymbol{i}_s^s \tag{26}$$

Even for low rotor speeds this drift compensation will only have a small effect on the magnitude and no effect on the orientation of $\boldsymbol{\psi}_\Delta^s$.

The linear estimation scheme derived in this section is shown in Fig. 5.

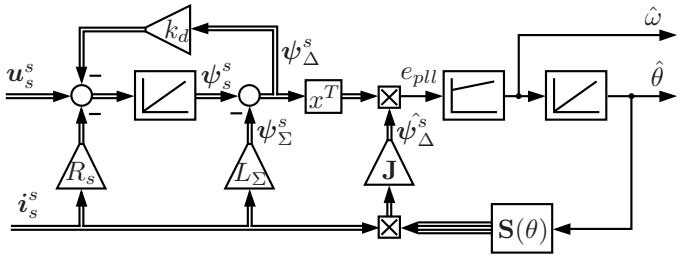

Fig. 5. Linear Estimation Scheme

V. Nonlinear Extension of the Estimation Scheme

The estimation scheme was derived assuming that the dependency of the flux linkage on the currents in rotor fixed frame is linear. As can be seen from Fig. 6 the flux linkage

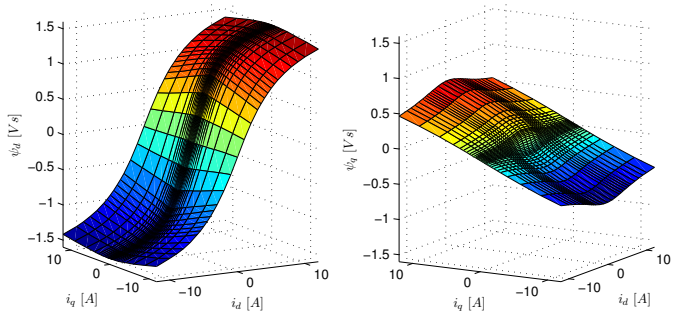

Fig. 6. Measured dependencies $\psi_d(i_d, i_q)$ and $\psi_q(i_d, i_q)$ of the flux linkage on the currents in rotor fixed frame

curves of the real machine show strong effects of saturation and cross saturation. The derived linear estimation scheme yields only bad results under these conditions.

A. Nonlinear Isotropic Flux Component

Nevertheless the main effects which the estimation scheme is based on are available also in the nonlinear case. The most important issue to solve in order to ensure stable behaviour, is to always find the centre of the flux circulation by accurate estimation of the vector $\boldsymbol{\psi}_\Sigma^s$. Therefore $\boldsymbol{\psi}_\Sigma^s$ still has to be isotropic but now a nonlinear function of the current. Such a nonlinear relationship can for instance be stored in a lookup table.

$$\boldsymbol{\psi}_\Sigma^s(\boldsymbol{i}_s^s) = \frac{\psi_d(|\boldsymbol{i}_s^s|, 0) + \psi_q(0, |\boldsymbol{i}_s^s|)}{2} \frac{\boldsymbol{i}_s^s}{|\boldsymbol{i}_s^s|} \tag{27}$$

$$= \psi_\Sigma(|\boldsymbol{i}_s^s|) \frac{\boldsymbol{i}_s^s}{|\boldsymbol{i}_s^s|} \tag{28}$$

Equation (27) and Fig. 7 describe how a lookup table for the isotropic flux component $\boldsymbol{\psi}_\Sigma^s$ is obtained from the flux curves of Fig. 6.

B. Angle Compensation

Once the isotropic flux component $\boldsymbol{\psi}_\Sigma^s$ is pointing to the centre it can be subtracted from the measured flux $\boldsymbol{\psi}_s^s$ (obtained by integration) in order to get the circulating salient component $\boldsymbol{\psi}_\Delta^s$. Though, as shown in Fig. 8, in the nonlinear

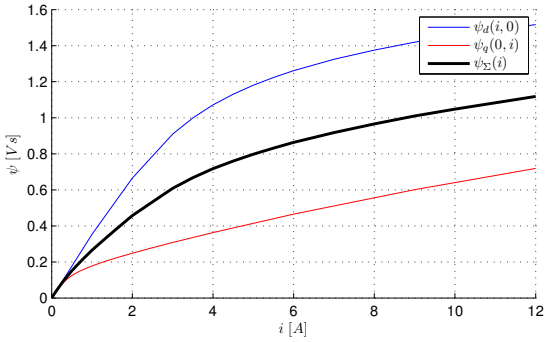

Fig. 7. Nonlinear magnitude of isotropic flux component $\boldsymbol{\psi}_\Sigma^s$

case $\boldsymbol{\psi}_\Delta^s$ does not run on a circle anymore. During the circulation it varies in magnitude and what is more important is that its angle differs in from the ideal circular path. Thus if

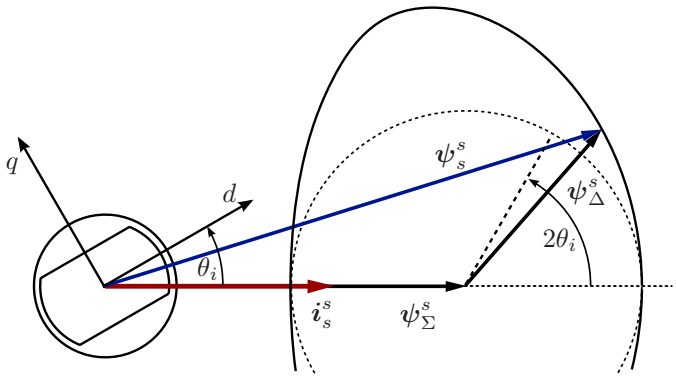

Fig. 8. Nonlinear circulation of the flux linkage ψ

the orientation of the measured $\boldsymbol{\psi}_\Delta^s$ is reconstructed correctly by (23) it must have been done using a wrong angle, which consequently leads to an estimation error in the proposed PLL based estimation scheme.

However, since this error is a function of the current and the current reference is a one dimensional signal it was possible to create a motor specific one dimensional compensation curve that is used to add a certain value to the estimated angle before calculating (23).

$$\theta_+ = sign(i^*)(0.23 - 0.002(|i^*|/A - 9)^2)rad \tag{29}$$

Thus, if the input error of the PLL and of the current controller is zero, also the angle $\hat{\theta}$ will be estimated correctly.

The compensation curve, indicated in Fig. 9, can be calculated out of the flux curves of Fig. 6 or simply be measured using a position sensor.

Concluding these adoptions for the nonlinear circumstances, the entire estimation scheme is indicated in Fig. 10.

VI. Measurement Results

The proposed nonlinear estimation scheme has been investigated for an RSM with the following properties.

As indicated in Fig. 11 the investigated RSM is coupled via a torque sensor to an induction machine as load. Each machine

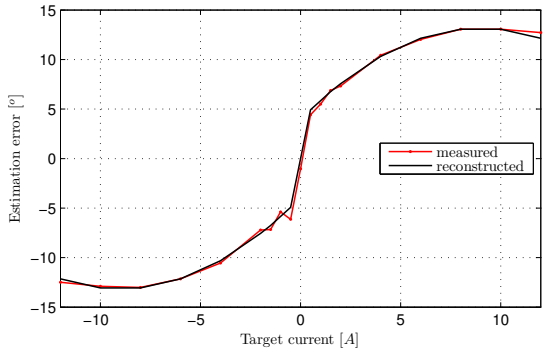

Fig. 9. Dependency of the angle estimation error on the target current

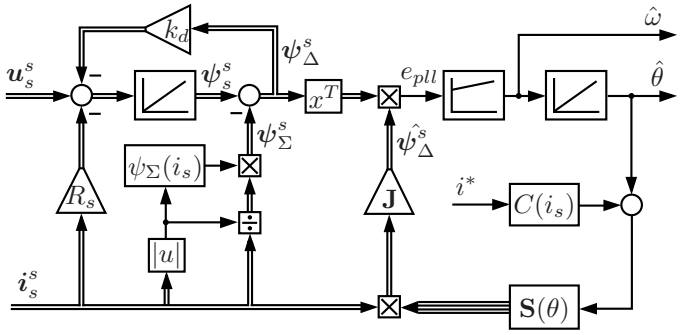

Fig. 10. Nonlinear Estimation Scheme

is driven by a $5kW$ inverter and controlled by a PC based real time system. Using this setup first the stationary and then the dynamic behaviour of the closed loop estimation scheme is evaluated.

As indicated in Fig. 12 for speeds above $40rad/s$ the proposed scheme is able to estimate properly even for three times nominal torque. This upper torque limitation was given by the maximum current of the inverter. The quick torque drop for speeds above base speed is due to the suboptimal properties of the RSM and of the torque control method in the field weakening area. However, these limitations are not caused by the estimation scheme.

Fig. 12 also shows that below $40rad/s$ the torque must be decreased: as known for fundamental model based estimation schemes, also this scheme tends to become unstable for low speeds, due to parameter errors and drift effects. It can be seen that approximately 10% of the rated speed is necessary

Pole pairs	2	
Nominal power	1.1	kW
Rated current	3.5	A
Rated mechanical torque	7	Nm
Rated electrical speed	314	rad/s

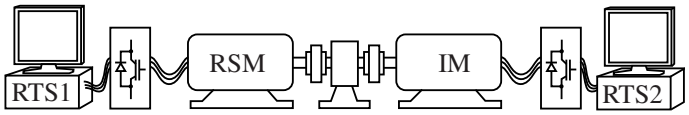

Fig. 11. Experimental Setup

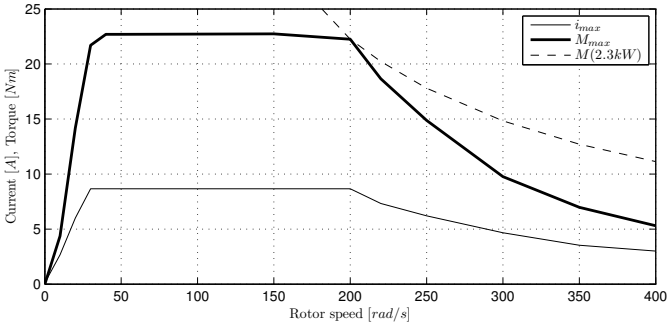

Fig. 12. Region of stable stationary closed loop control

for stable closed loop control at nominal torque. Further work could be focused on lowering this limit for instance by implementing a resistance estimation scheme or by a combination with a high frequency injection based position estimation scheme.

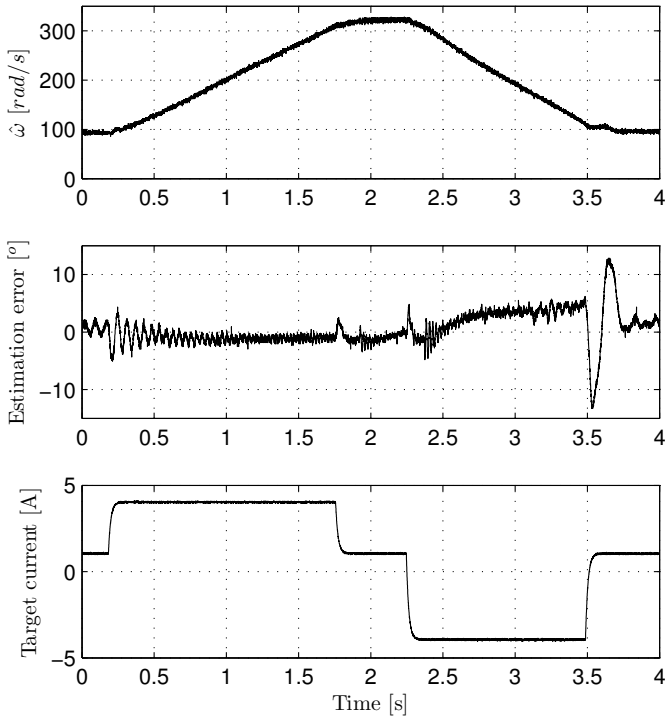

Fig. 13. Dynamic characteristics in current control

Fig. 13 shows the results of the first dynamic measurement. Starting from $\omega = 100rad/s$ constant speed the RSM accelerates a emulated inertia with $M = 8Nm$ up to $\omega = 300rad/s$ and decelerates down to $\omega = 100rad/s$ again. The oscillation at the beginning of the measurement is noticed and conclusions are drawn later. Despite using a compensation curve the decelerating period brings up a constant estimation error of approximately 3.5^o whose cause is not clarified yet.

Furthermore the estimation error shows a sensitivity to current gradients, which particularly becomes strong at low speeds and low currents when the PLL input signal is less

significant. This results in the two stronger peaks of the estimation error at the end of the decelerating period. But since under these conditions almost no torque is required the peaks have hardly any effect on the outer behaviour of the machine.

In the second dynamic experiment the RSM is driven sensorless speed controlled at $250rad/s$ and two steps in the target speed of $\pm 50rad/s$ are applied. As can be seen from Fig. 14 the very steep gradients in target current, which are fed through the speed controller, do only hardly affect the estimation error.

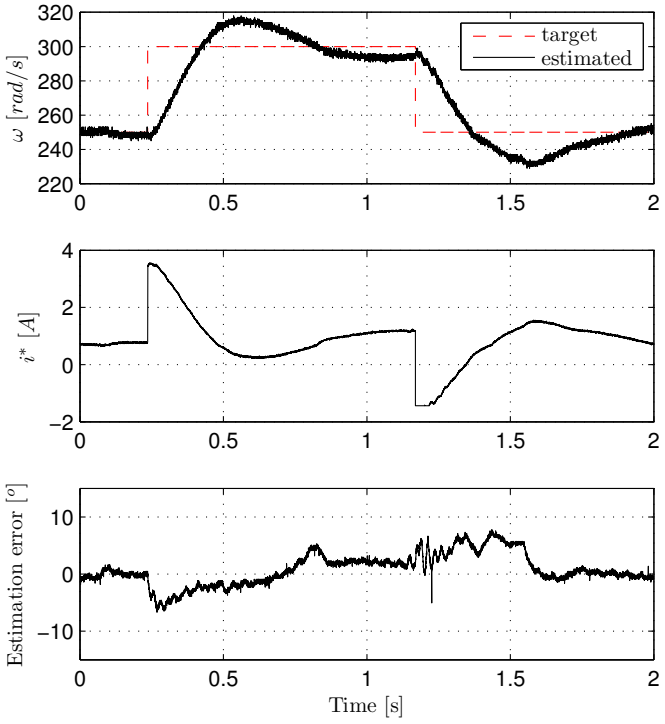

Fig. 14. Response to speed reference step in speed control

In the last dynamic experiment the RSM is driven sensorless speed controlled at $250rad/s$ and two steps in the load torque of $\pm 6Nm$ are applied. The response of the closed loop estimation scheme is shown in Fig. 15. Since the magnitude of the load torque is 85% nominal torque the target current needs to go into limitation. Since the frequency of the oscillation, which again appears under the condition of high currents, is equal to the electrical rotor speed it can be inferred that the PLL is tracking a slightly superimposed stator saturation caused saliency.

All in all the measurements are showing that the proposed approach, as one of the few fundamental sensorless methods for the RSM, yields quite convincing results and can be considered as a reliable component for medium to high speed in a hybrid sensorless control scheme.

VII. Conclusion

A new fundamental position estimation scheme for an RSM has been presented. As the RSM has no rotor own source of flux the scheme is based on the fundamental saliency. First a linear estimation scheme was derived in theory and then extended for the nonlinear effects in a real machine. Finally the performance of the proposed scheme was proved by stationary and dynamic measurements.

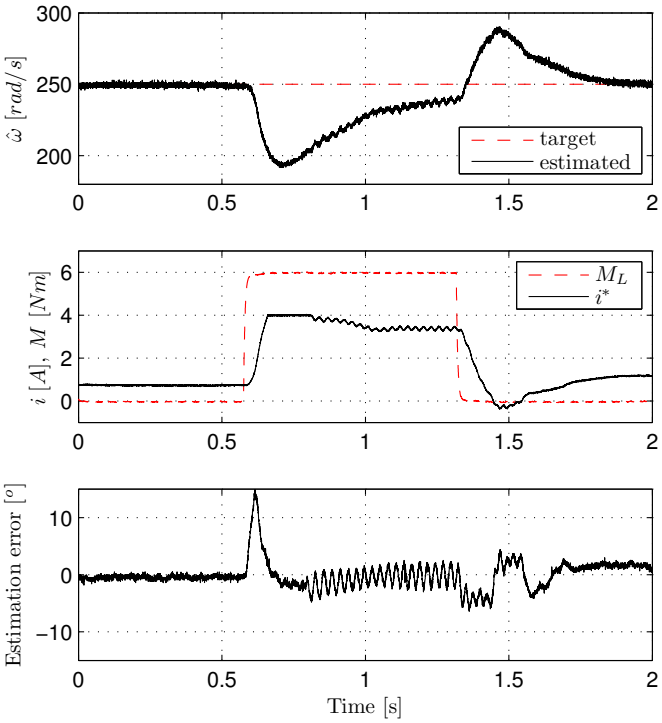

Fig. 15. Response to load torque step in speed control

References

[1] A. Consoli, G. Scarcella, G. Scelba, A. Testa, and D. A. Triolo, "Sensorless rotor position estimation in synchronous reluctance motors exploiting a flux deviation approach," *IEEE Trans. Industrial Appl.*, vol. 43, pp. 1266–1273, 2007.

[2] H. F. Hofmann, S. R. Sanders, and A. EL-Antably, "Stator-flux-oriented vector control of synchronous reluctance machines with maximized efficiency," *IEEE Trans. on Industrial Electronics*, vol. 51, pp. 1066–1072, 2004.

[3] G. Pellegrino, E. Armando, P. Guglielmi, and A. Vagati, "A 250kw transverse-laminated synchronous reluctance motor," *EPE Conf*, vol. 1, pp. 1–10, 2009.

[4] P. L. Jansen and R. D. Lorenz, "Transducerless position and velocity estimation in induction and salient ac machines," *IEEE Trans. Industrial Appl.*, vol. 31, pp. 240–247, 1995.

[5] M. J. Corley and R. D. Lorenz, "Rotor position and velocity estimation for a salient-pole permanent magnet synchronous machine at standstill and high speeds," *IEEE Trans. Industrial Appl.*, vol. 34, pp. 784–789, 1998.

[6] M. Linke, R. Kennel, and J. Holtz, "Sensorless speed and position control of synchronous machines using alternating carrier injection," *IEMDC Conf.*, vol. 2, pp. 1211– 1217, 2003.

[7] J. Jang, S. Sul, J.-I. Ha, K. Ide, and M. Sawamura, "Sensorless drive of surface-mounted permanent-magnet motor by high-frequency signal injection based on magnetic saliency," *IEEE Trans. Industry Application*, vol. 39, pp. 1031– 1039, 2003.

[8] M. Schroedl, "Sensorless control of ac machines at low speed and standstill based on the "inform" method," *IEEE Trans. Industrial Appl.*, vol. 34, pp. 270–277, 1996.

[9] R. Morales-Caporal and M. Pacas, "Encoderless predictive direct torque control for synchronous reluctance machines at very low and zero speed," *IEEE Trans. on Industrial Electronics*, vol. 55, p. 4408, 2008.
[10] R. Wu and G. Slemon, "A permanent magnet motor drive without a shaft sensor," *IEEE Trans. Industrial Appl.*, vol. 27, pp. 1005–1011, 1991.
[11] T. Furuhashi, S. Sangwongwanich, and S. Okuma, "A position-and-velocity sensorless control for brushless dc motors using an adaptive sliding mode observer," *IEEE Trans. on Industrial Electronics*, vol. 39, pp. 89–95, 1992.
[12] S. Ichikawa, M. Tomita, S. Doki, and S. Okuma, "Sensorless control of synchronous reluctance motors based on extended emf models considering magnetic saturation with online parameter identification," *IEEE Trans. Industrial Appl.*, vol. 42, pp. 1264–1274, 2006.
[13] R. Lagerquist, I. Boldea, and T. J. E. Miller, "Sensorless control of the synchronous reluctance motor," *IEEE Trans. Industrial Appl.*, vol. 30, pp. 673–682, 1994.
[14] E. Capecchi, P. Guglielmi, M. Pastorelli, and A. Vagati, "Position-sensorless control of the transverse-laminated synchronous reluctance motor," *IEEE Trans. Industrial Appl.*, vol. 37, pp. 1768–1776, 2001.
[15] H. de Kock, M. Kamper, and R. Kennel, "Anisotropy comparison of reluctance and pm synchronous machines for position sensorless control using hf carrier injection," *IEEE Trans. Power Electronics*, vol. 24, pp. 1905–1913, 2009.